

AN ABSTRACT OF THE THESIS OF

Mark Bernard Siddall for the M. S. in Material Science
(Name) (Degree) (Major)

Date thesis is presented December 4, 1964

Title SUPER CONDUCTIVE A. C. LOSSES AS A FUNCTION OF AN
APPLIED STEADY MAGNETIC FIELD IN TYPE II SUPER-
CONDUCTORS

Abstract approved

Redacted for Privacy

(Major professor)

Measurements were made of the energy loss in a superconducting wire coil subjected to an axial magnetic field consisting of a ripple field superimposed on a steady field. The loss was measured calorimetrically using a sonic thermometer consisting of a resonance tube filled with helium gas in thermal contact with the superconducting wire under test. An adiabatic calorimeter and an almost isothermal calorimeter were constructed to measure the losses and their respective results were compared. The critical state theory of Kim, Hempstead and Strnad predicts the experimentally determined loss characteristics. The loss-vs-steady field characteristic was measured for Niobium, 25 wt percent Zirconium, 10 MIL wire. General agreement with Kim's theory was found with a maximum loss occurring at 254,000 ampere-turns per meter, such loss falling to a lower and constant value at fields above 795,000 ampere-turns per meter.

SUPERCONDUCTIVE A. C. LOSSES AS A
FUNCTION OF AN APPLIED STEADY MAGNETIC FIELD
IN TYPE II SUPERCONDUCTORS

by

MARK BERNARD SIDDALL

A THESIS

submitted to

OREGON STATE UNIVERSITY

in partial fulfillment of
the requirements for the
degree of

MASTER OF SCIENCE

June 1965

APPROVED:

Redacted for Privacy

Associate Professor of Electrical Engineering

In Charge of Major

Redacted for Privacy

Head of Department of Electrical Engineering

Redacted for Privacy

Dean of Graduate School

Date thesis is presented December 4, 1964

Typed by Carol Baker and Eula Weathers

ACKNOWLEDGEMENTS

It is a pleasure to thank Professor J. F. Engle for advice and assistance, Professor O. G. Paasche for encouragement, and S. W. H. Yih of Wah Chang Corporation, Albany, Oregon for support.

TABLE OF CONTENTS

	<u>Page</u>
INTRODUCTION	1
THEORY	3
Relation of Magnetization Curve to Heat Energy Generation	7
EXPERIMENTAL	13
Adiabatic Calorimeter	13
Almost Isothermal Calorimeter	19
RESULTS	27
Theoretically Predicted Heat Loss Calculation	27
Almost Isothermal Calorimeter	27
Adiabatic Calorimeter	31
CONCLUSIONS	34
RECOMMENDATIONS	35
BIBLIOGRAPHY	36

LIST OF FIGURES

<u>Figure</u>		<u>Page</u>
1	Magnetization Curves after Kim <u>et al.</u> (7)	8
2	Theoretical Heat Loss as a Function of Field for Sample Tube H.	12
3	Experimental Set-up.	14
4	Schematic of Apparatus.	15
5	Calorimeters.	16
6.	Heat Loss-versus-Field Comparison of Theory and Experiment.	32

LIST OF TABLES

<u>Table</u>		
1	Adiabatic Calorimeter Data.	20
2	Quench Currents of Spot Welded and Cold Worked Joints in Nb 25Zr Wire.	23
3	Temperature and Pressure Calibration of Almost Isothermal Calorimeter [Compared with Data of Van Itterbeek <u>et al.</u> (11)] .	25
4	Temperature Rise of Almost Isothermal Calorimeter Due to Standard 10 KC Input.	26
5	Magnetization Data from Kim <u>et al.</u>	27
6	Alternating Field Energy Loss-versus-Magnetic Field	28
7	Almost Isothermal Calorimeter	29
8	Heat Losses for Almost Isothermal Calorimeter	30
9	Heat Losses for Adiabatic Calorimeter	31

LIST OF SYMBOLS

Symbol	Quantity	Units Employed (MKS)
H _c	Lower critical field strength for flux penetration	$\frac{\text{AMP-TURN}}{\text{METER}}$
J _c	Filamentary critical current density	$\frac{\text{AMP}}{\text{METER}^2}$
B	Magnetic flux density	$\frac{\text{WEBER}}{\text{METER}^2}$
J	Current density	$\frac{\text{AMP}}{\text{METER}^2}$
H	Field intensity	$\frac{\text{AMP-TURN}}{\text{METER}}$
m	Magnetic polarization	$\frac{\text{WEBER}}{\text{METER}^2}$
c	A constant, of value :	$3. \times 10^8$
a	Outer radius of super- conducting cylinder specimen	METER
x	Radius variable	METER
r	Radius variable of super- conducting mixed state	METER
w	Wall thickness of super- conducting tube	METER
H'	Field intensity inside tube sample	$\frac{\text{AMP-TURN}}{\text{METER}}$
M	M = H - H' , Magnetization	$\frac{\text{AMP-TURN}}{\text{METER}}$
H ₀	Lower critical field intensity	$\frac{\text{AMP-TURN}}{\text{METER}}$
a	A constant, of units	$\frac{\text{AMP}^2\text{-TURN}}{\text{METER}^3}$

LIST OF SYMBOLS(CONTINUED)

h	$h = H/H_0$	DIMENSIONLESS
h'	$h' = H'/H_0$	DIMENSIONLESS
A	$A = 2a w/H_0^2$	DIMENSIONLESS
λ	Magnetic flux linkages	WEBER-TURNS
i_n	Current of normal electrons	AMPERE
L	Inductance	HENRY
R	Resistance	OHM
T	Time interval	SECOND
t	Time variable	SECOND
i_s	Current due to super-conducting electrons	AMPERE
W	A. C. power loss in super-conductor	WATT
f	means : 'function of'	
KOe	means : 10^3 Oersteds	
K_p	Thermal conductivity	$\frac{\text{WATTS}}{\text{CM-DEGREE}}$
$^{\circ}\text{K}$	Degrees Kelvin	
$\delta \rho$	Resistivity	OHM-METER
n_s	Number of turns, secondary	
n_p	Number of turns, primary	
d_p	Diameter of winding, primary	METER
d_s	Diameter of winding, secondary	METER
ΔP	Change of pressure	$\frac{\text{NEWTON}}{\text{METER}^2}$

SUPERCONDUCTIVE A. C. LOSSES AS A FUNCTION OF AN APPLIED STEADY MAGNETIC FIELD IN TYPE II SEMICONDUCTORS

INTRODUCTION

Magnetization measurements have provided important data for the elucidation of characteristics of non-ideal superconductors. The non-reversibility of magnetization observed in high defect density specimens has been attributed variously to at least one of the following theories: 1) flux filament motion through a matrix of deformation or impurity induced pinning centers (3, 7) or , 2) non-reversible thermodynamic interactions of superconducting lamina with pinning centers (1, 6, 10). In either case the non-reversibility observed in the alternating field properties of plastically deformed Type II superconductors should be observable in terms of the heat gain of an isolated gas system containing the superconductor under the influence of a magnetic field.

The heat gain of such a system was measured by the temperature rise of the system by a method that was independent of ambient magnetic fields. This procedure made use of a sonic thermometer using helium gas in thermal contact with the superconductor under test (11).

Calculations indicate that the heat sensitivity of this method should be comparable to the measurement of the a - c losses with an

inductance bridge (12). Ballistic temperature shift and equilibrium temperature shift methods were both tried. The steady measurements of equilibrium were easiest to calibrate and measure because they depend only on heat transfer coefficients and not on the variable specific heat.

Comparison of measured heat loss with field penetration is made by differentiating the field penetration curve. This allows a comparison with the predictions of the critical state theory of Kim, Hempstead and Strnad (3) following Bean (4), which states that the heat generation is the greatest where the field penetration curve has the steepest slope.

THEORY

Hard superconductors display superconducting properties in fields much greater than the critical fields of soft superconductors. When a high defect density is introduced into a hard superconductor the critical current at high fields is increased greatly, but the losses due to alternating current magnetic fields also increase. The application of the Ginsburg, Landau, Abrikosov, Gorkov (GLAG) theory (1, 5) to high defect density superconductors therefore seems to require a modification to take into account the interaction of the flux pinning centers with the otherwise thermodynamically reversible superconducting lamina (2, 4, 10).

Magnetization and specific heat measurements have been extensively used to establish the nature of this interaction and the objective of this thesis is to verify the magnetization experiments with respect to field intensity. A description of the critical state theory of magnetization by Bean (3) and Kim et al. (7) indicates that the square of the slope of the magnetization curve is proportional to the energy loss in heat.

This theory is an alternative to the GLAG theory. The critical state theory follows the hypothesis first put forth by Mendelssohn (8) who proposed a hard superconductor model consisting of a filamentary mesh network of high field superconductors in a matrix of

soft superconducting material.

Bean (3) derives magnetization curves for a cylindrical superconductor of the filamentary type as a function of the soft superconductor critical field--and the radius of the cylinder. The magnetization curves are derived for the cases where: 1) a parallel field is excluded from the superconductor at low fields; 2) there is partial field penetration for the filamentary state in the outer shell of the cylinder; 3) complete penetration occurs where the entire cylinder is in the mixed state of superconducting filaments in a matrix of normally conducting metal.

Bean's magnetization experiments with sintered Nb_3Sn cylinders followed closely the predicted curves by fitting to $H_c = 159,000$ amp-turns per meter and $J_c = 1.2 \times 10^9 \frac{\text{amps}}{\text{m}}$.

Niobium is in the interstices of the Nb_3Sn filament structure.

The value of H_c measured for niobium by quench current tests is 0.2 Weber per square meter. This provides confirmation of his theory.

Kim, Hempstead and Strnad extend this work (3) by assuming that the superconducting regions are all at the limit of their current carrying ability for the value of field at any location. This allows a calculation of a unique critical current density $J(B)$ for each value of flux density B , by using the relations in MKS units

$$\vec{B} = \mu_0(\vec{H} + \vec{M}) \quad (1)$$

$$\vec{J}(B) = \nabla \times \vec{M} \quad (2)$$

when the magnetic field intensity H is given.

For an infinitely long cylinder of outer radius a , to which a parallel external field intensity H is applied, Equations reduce to a scalar equation

$$\begin{aligned} B(r) &= \mu_0(H + M(r)) \\ &= \mu_0 H + \mu_0 \int_r^a J(H(x)) dx. \end{aligned} \quad (3)$$

In this equation x and r are radial variables in terms of m .

Solving for an integral over H using:

$$M(r) = \int_r^a J(H(x)) dx \quad (4)$$

$$M = J(a-r) \text{ at a given } H. \quad (5)$$

The integral over H is, using the identity

$$M(r) = \int_H^{H+M(r)} dH \quad (6)$$

$$(a-r) = \int_H^{H+M(r)} \frac{dH}{J(H)} \quad (7)$$

To apply this equation to a tubular sample of wall thickness w , where $w = a - r$, the field intensity H' , measured inside the tube, is made the inner boundary of the integral

$$w = \int_{H'}^H \frac{dH}{J(H)} \quad (8)$$

The functional dependence of $J(H)$ is determined experimentally. Log-log plots of magnetization M (where $M = H - H'$) - versus-average H give straight lines of slope -1 . The distribution is then

$$a/J = H_0 + H \quad (9)$$

where a and H_0 are constants.

Substitution of Equation (9) into Equation (8) gives

$$\begin{aligned} -w &= \int_H^{H'} \frac{H_0 + H}{a} dH \\ &= \frac{H_0}{a} (H' - H) + \frac{1}{a} \frac{H^2}{2} \Bigg|_H^{H'} \\ &= \frac{1}{a} \left[H_0 H' - H_0 H + \frac{H'^2}{2} - \frac{H^2}{2} \right] \\ -a \cdot w &= (H' - H) \left[H_0 + \frac{H'}{2} + \frac{H}{2} \right] \\ \frac{-a \cdot w}{H - H'} &= H_0 + \frac{1}{2} (H' + H) \quad (10) \end{aligned}$$

Using the notation

$$H/H_0 = h, \quad H'/H_0 = h', \quad A \equiv \frac{2a \cdot w}{H_0^2}$$

Kim, et al. obtains

$$\begin{aligned} -\frac{2a \cdot w}{H_0^2} \equiv A &= \frac{[H_0 + \frac{1}{2}(H' + H)](H - H')^2}{H_0^2} \\ \pm A &= \left[\frac{H_0}{H_0} + \frac{1}{2} \left(\frac{H'}{H_0} + \frac{H}{H_0} \right) \right] \left(\frac{H}{H_0} - \frac{H'}{H_0} \right)^2 \\ &= \left[1 + \frac{1}{2}(h' + h) \right] (H - h')^2 \\ &= 2(h - h') + (h^2 - h'^2) \\ \pm A &= (h' + 1)^2 - (h + 1)^2 \end{aligned} \tag{11}$$

This is a hyperbola where $-A$ is used for $H > H' > 0$ and $+A$ is used for $H' > H > 0$. In the case $H < 0 < H'$ a circle is obtained:

$$A + 2 = (h' + 1)^2 + (1 - h)^2 \tag{12}$$

Figure 1 shows these field intensity penetration curves from Kim et al. (7, p. 534). Note that the hyperbola and circle curves can be fitted well to the data points.

Relation of Magnetization Curve to Heat Energy Generation

When the critical state is reached, superconducting electrons will no longer be able to take up the acceleration of a changing

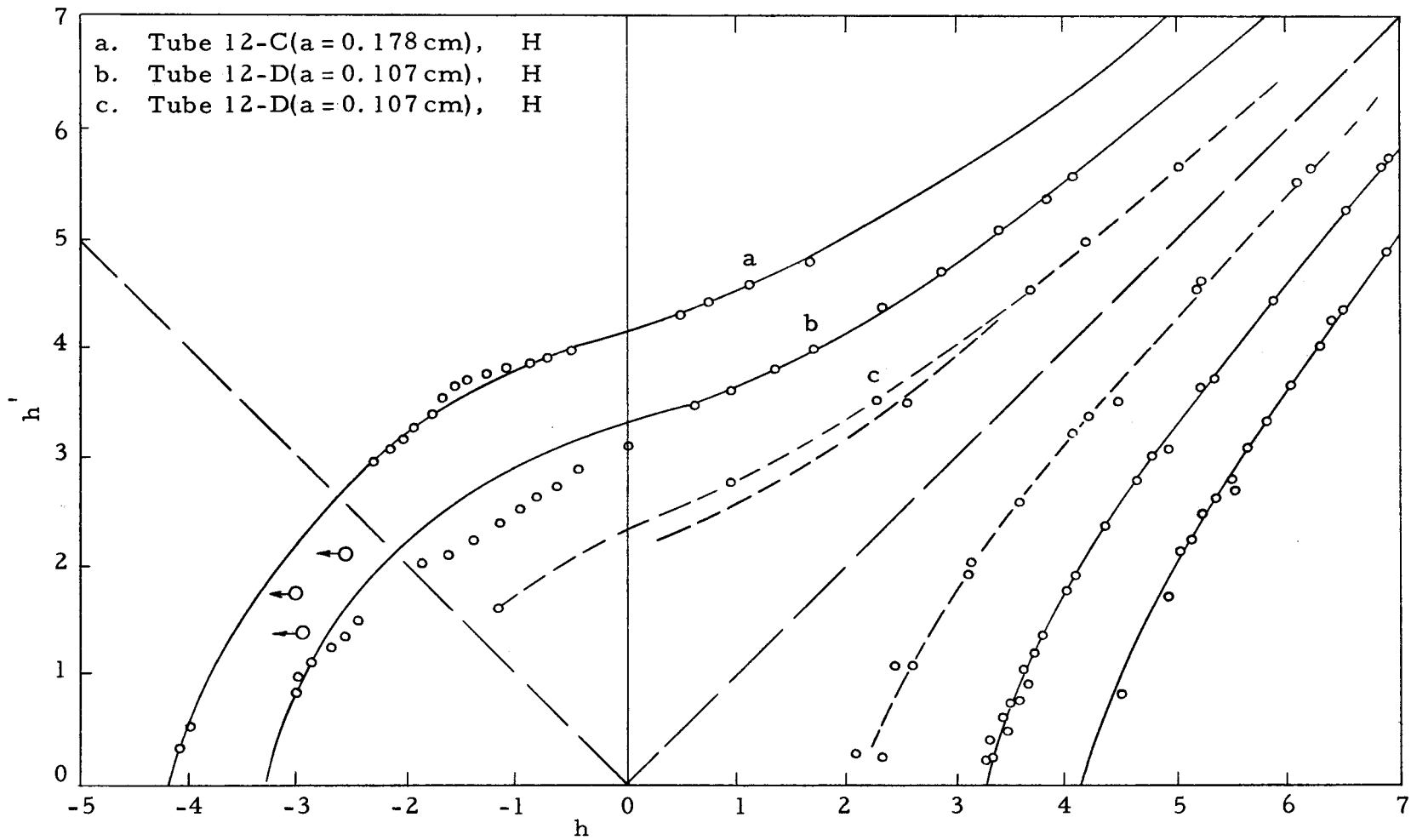


Figure 1. Field Intensity Penetration Curves after Kim et al. (7).

magnetic field and the normal electrons will be accelerated in the following way:

$$\frac{d}{dt}(Li_n + \lambda) = i_n R \quad (13)$$

λ is the external flux linkages seen by the normal current and due to the external field intensity H and the supercurrent i_s .

λ is now changed from λ_1 to λ_2 uniformly over a period T . In this case i_n builds up to a maximum value at $t = T$ and then gradually decays with a time constant $t = L/R$. The heat energy generated by i_n is given by

$$W = \frac{(\lambda_1 - \lambda_2)^2}{L} f\left(\frac{T}{t}\right) \quad (14)$$

For a thin walled cylinder of radius a , λ is given approximately by

$$\lambda = 4\pi^2 H' a^2 \times 10^{-7} \quad (15)$$

$$\Delta\lambda = \lambda_2 - \lambda_1 = 4\pi^2 a^2 \times 10^{-7} \Delta H' \quad (16)$$

Thus for a given external field change ΔH with a given rate of change $\Delta H/T$,

$$W \approx \left(\frac{dH'}{dH}\right)^2 \quad (17)$$

The above equation indicates that the heat generation is

proportional to the square of the slope of the h' versus h curve, where h' is the field intensity inside the cylinder.

To calculate the shape of this heat generation curve, the derivative of Kim's expression for the hyperbola and circle should be squared. This derivative is shown below,

$$(h' + 1)^2 - (h + 1)^2 = \pm A \quad (11)$$

$$(d/dh)[(h' + 1)^2] - (d/dh)[(h + 1)^2] = (d/dh)[\pm A] \quad (18)$$

$$2(h' + 1)(dh'/dh) - 2(h + 1) = 0$$

$$dh'/dh = (h + 1)/(h' + 1)$$

Now using the equality $(h' + 1)^2 = \pm A + (h + 1)^2$ from Equation (11),

$$(dh'/dh) = \frac{h + 1}{\sqrt{\pm A + (h + 1)^2}} \quad (19)$$

Equation (19) squared gives the following:

$$(dh'/dh)^2 = [(h + 1)^2] / [\pm A + (h + 1)^2] ; \quad (20)$$

for $A = 0$, i. e., thin wall or for $h \gg A$ the slope is a constant = 1. Note the pole appearing at $A = -(h + 1)^2$.

Similarly for the circle:

$$(h' + 1)^2 + (1 - h)^2 = A + 2 \quad (21)$$

$$(d/dh)[(h' + 1)^2] + (d/dh)[(1-h)^2] = (d/dh)(A+2) \quad (22)$$

$$2(h' + 1) dh'/dh - 2(1 - h) = 0$$

$$dh'/dh = (1 - h)/(h' + 1)$$

Substituting $(h' + 1)^2 = A + 2 - (1-h)^2$ from Equation (12),

$$dh'/dh = \frac{1-h}{\sqrt{A+2-(1-h)^2}} \quad (23)$$

Squaring the slope Equation (23) gives the following:

$$(dh'/dh)^2 = [(1-h)^2] / [A+2-(1-h)^2]$$

Here again the slope approaches a constant value 1 when $h \gg A$.

Where $h \sim A$ there is a transition, with a pole at $A = \frac{(1-h)^2}{2}$.

The curve of $(dh'/dh)^2$ - versus- h is plotted as Figure 2.

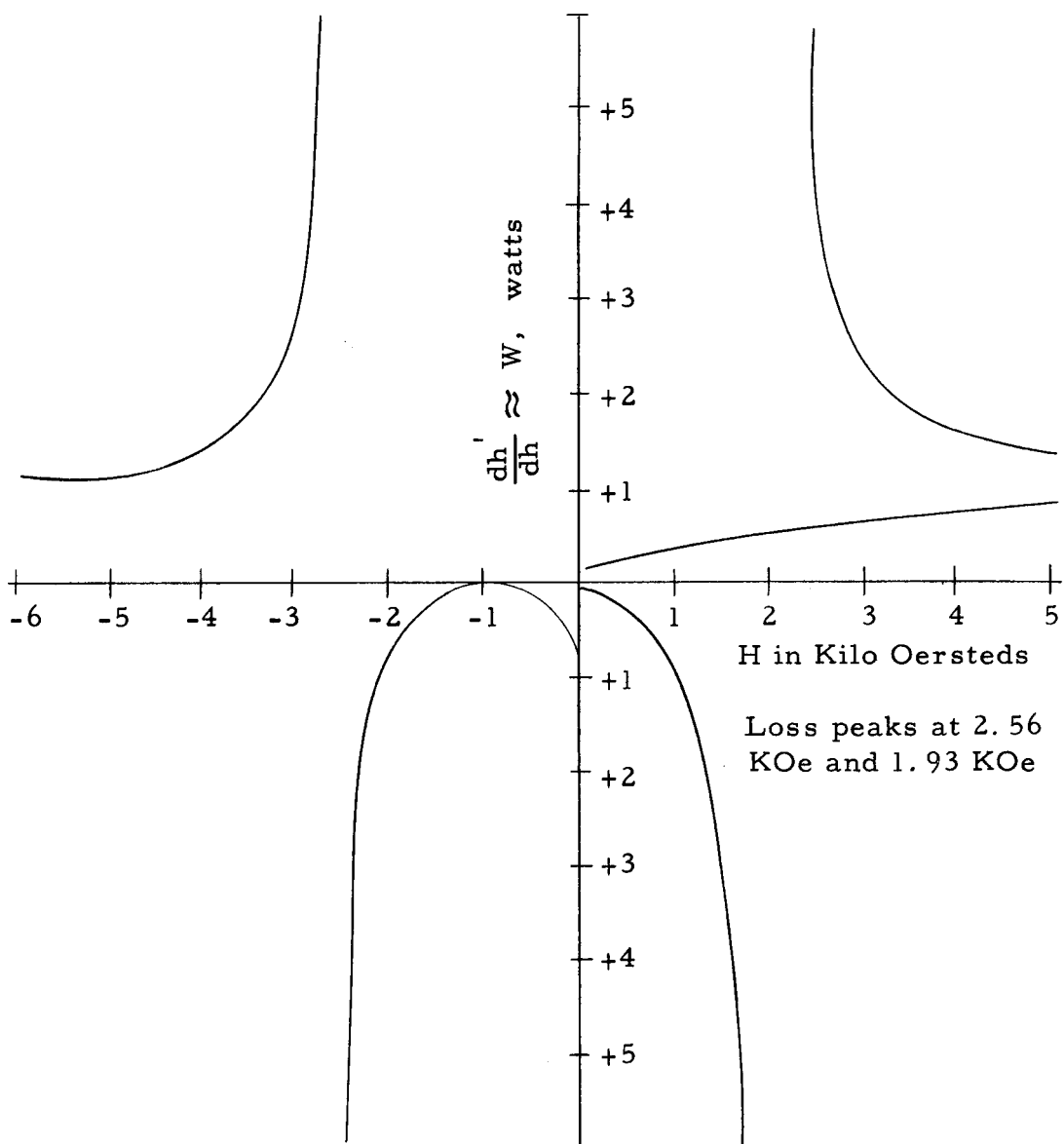


Figure 2. Theoretical Heat Loss as a Function of Field for Sample Tube H.

EXPERIMENTAL

Several forms of calorimeter were constructed for the thermal measurements. All calorimeters were designed to be inserted into the 0.40 inch bore of a superconducting magnet capable of producing a field of 50,000 oersteds when cooled by liquid helium.

Electromagnetic cgs units are used in the following experimental and results sections of this thesis. These units were used because of the factory calibration and existing scales on equipment and the previous experience of the author.

Figure 3 is the over-all experimental equipment showing left to right: helium storage dewar with calorimeter probe inserted for pre-cooling, experimental dewar containing superconducting magnet, vacuum controls (behind experiment), electronic equipment for operation of sonic thermometer and for application of the alternating field, and on the right the magnet power supply.

Figure 4 is a schematic diagram of the experimental circuit including sonic thermometer and power supplies for a-c excitation of sample.

Figure 5 shows the design of the adiabatic calorimeter and the nearly isothermal calorimeter.

Adiabatic Calorimeter

The adiabatic calorimeter consists of a closed loop winding of the test superconducting wire mounted on a thermally isolated pyrex spindle. A primary winding concentric to the test winding and wound on the outside of the outer tube is connected to an external a-c source.



Figure 3. Experimental Set-up.

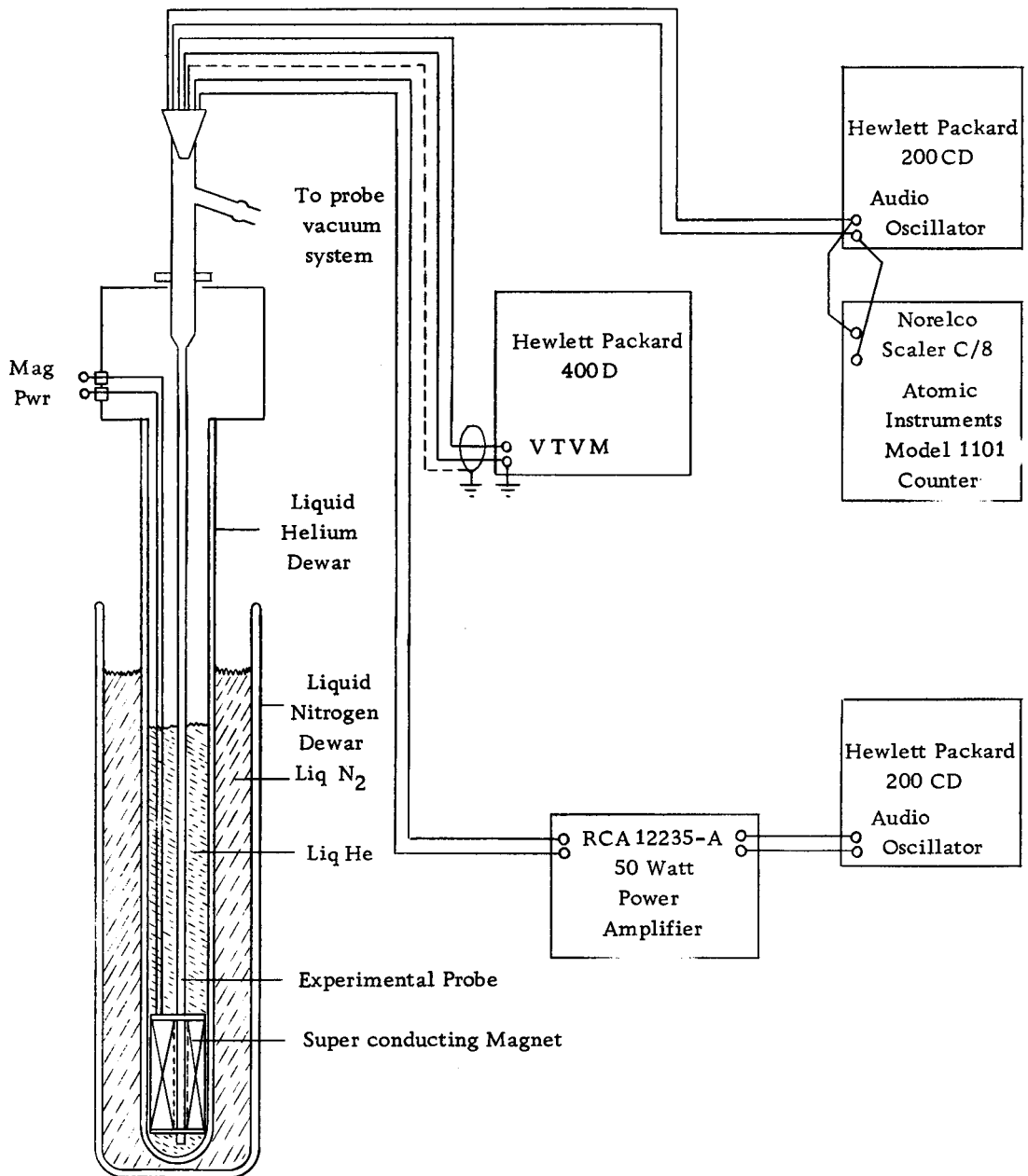


Figure 4. Schematic of Apparatus.

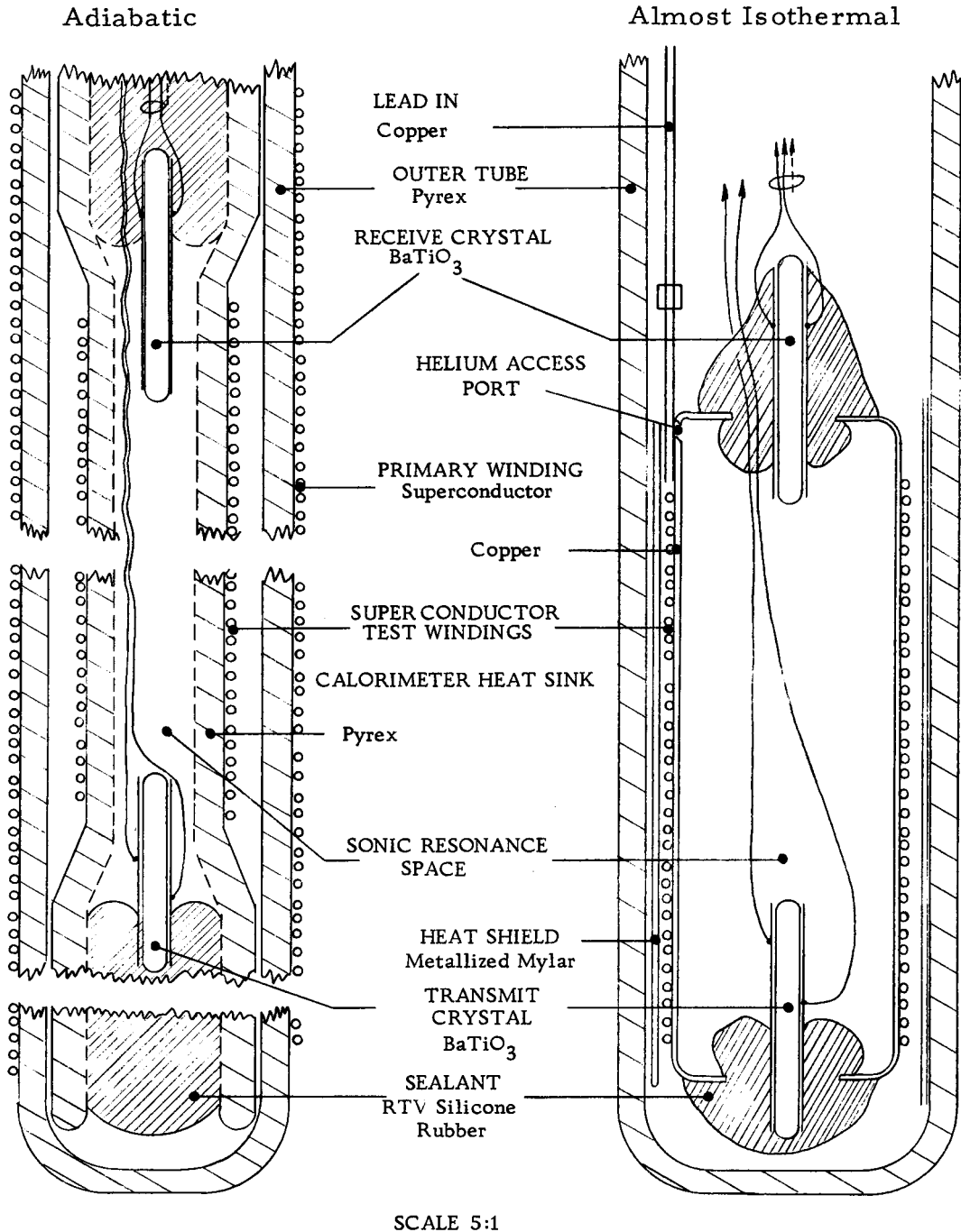


Figure 5. Calorimeters.

Transformer action excites the secondary winding. Helium gas sealed in the central cavity provides the medium for the sound from a barium titanate phonograph crystal to be carried to a similar crystal acting as the sound detector.

The speed of sound in the tube can be determined by measuring the resonant frequency of the tube with a counter when the distance between the crystals is known.

In operation, the outer tube is pumped out with a mechanical vacuum pump, then cooled in liquid helium. The helium freezes out the remaining air and provides thermal isolation for the calorimeter spindle. End loss of heat through the pyrex becomes small as the temperature approaches absolute zero. The thermal conductivity of pyrex, K_p , is given as follows:

$$K_p @ 273^{\circ}\text{K} = 10.2 \left(\frac{\text{milliwatts}}{\text{CM-Deg}} \right)$$

$$K_p @ 4.2^{\circ}\text{K} = 1 \left(\frac{\text{milliwatts}}{\text{CM-Deg}} \right)$$

The specific heat of the pyrex becomes small as the temperature nears zero^oK, and thus heat sensitivity of the apparatus increases by at least three orders of magnitude due to low temperature effects. The value of constant power loss in the super conductor necessary to raise the temperature by 0.1^oK in a one minute time period is determined as follows; this is equivalent to a 0.25 percent resonant

frequency change in the sound cavity at 4.2°K (11, p. 63).

Weight of spindle ≈ 1 gm.

$$\begin{aligned}\Delta W &= 0.01 \left(\frac{\text{cal}}{\text{mol}^{\circ}\text{C}} \right) \left(\frac{1 \text{ mol}}{25\text{g}} \right) \left(\frac{1 \text{ watt sec}}{.239 \text{ cal}} \right) \left(\frac{1 \text{ min}}{60 \text{ sec}} \right) (.1^{\circ}\text{C}) = \\ &= 0.00028 \text{ watts}\end{aligned}$$

The heat loss in the 39 turns of Nb25Zr wire was calculated from data of J. L. Zar (12, p. 803) where an effective a-c resistance is plotted versus frequency for Nb-Zr alloys.

At 60 cycles/sec a resistivity, ρ , of 10^{-10} ohm-cm is measured while at 10,000 cycles/sec, $\rho = 9. \times 10^{-9}$ ohm-cm.

The calculation of the 60 cycles/sec current required to achieve a measurable power loss is as follows:

$$I = \sqrt{P/R} = \frac{.0028 \times 5.07 \times 10^{-4}}{\sqrt{10^{-10} \times 55.2 \text{ cm}}} = \sqrt{2.57 \text{ amps}^2} = 5.1 \text{ amps}$$

The existing winding outside the calorimeter must induce 5.1 amps RMS in the secondary. The primary current required is

$$I_p = I_s \left(\frac{n_s}{n_p} \right) \left(\frac{d_p^2}{d_s^2} \right),$$

for a long concentric solenoid of n turns and diameter, d .

$$I_p = 5(39/129) \left[\frac{(8.5)^2}{(4.5)^2} \right] = 53.8 \text{ amps}$$

The 0.25 percent change of frequency at 3600 cycles/sec results in a shift of 9. cycles/sec. Measurements of the oscillator stability shows a variation of ± 3 cycles/sec at 10. KC over a period of hours when the oscillator is in still air.

Therefore, we would expect to see a statistically measurable shift in frequency upon the application of an alternating field to the test wire.

Table 1 shows the data taken with the adiabatic calorimeter. Results are given in the results section. Note that currents less than 22.5 amps RMS give no measurable frequency shift.

The super conducting secondary loop was closed with a spot welded joint. Quench current versus external field data for similar spot-weld-limited wires are given in Table 2.

RTV silicone rubber and oil were used as heat sink connection material from superconductor to calorimeter spindle.

Almost-Isothermal Calorimeter

This apparatus is shown on the right hand side of Figure 5. It is designed to operate in an atmosphere of helium gas with reduced pressure inside the probe. Although inherently less sensitive than the adiabatic calorimeter, this device has better heat transfer from superconductor to helium gas, thus this method becomes more attractive for steady state measurements. A further advantage

TABLE 1
Adiabatic Calorimeter Data

Magnet Current (Amps)	Field (K Oe)	Counter			Time of Day	60 c/s AC current (22.5 A.rms)	Ave. Freq. (cy/sec)	Freq. Shift (cy/sec)
		Counts 8	Time (Seconds)	Freq. (cy/sec)				
0	0	3654	7.98	3660	7:22 pm	OFF	3656.0	
		3688	8.03	3687				
		3650	8.00	3650				
		36563	80.00	3656				
0	0	-	-	-	7:26 pm	ON	3665.0	
		3673	8.00	3673	7:30.00			
		3676	8.01	3676	7:31			
		3683	8.02	3682	7:32			
		3656	7.98	3657	7:33			
		3670	8.02	3669	7:34			
		36593	80.00	3661	7:35			
		3687	8.02	3686	7:36			
		-	-	-	7:37			
		3679	8.02	3678	7:38			
		3679	7.99	3680	7:39			
					7:41			
					7:42			
				OFF				
					COUNTER INTERVAL INCREASED			
		36636	80.04	3662	7:43		3662.0	
7.1	20	36556	80.00	3656	7:51		3657.0	
		36554	79.97	3657	7:53			
		-	-	-	7:55.40	ON		
7.1		36579	80.00	3660	7:58.40			
		36559	79.97	3657	7:60.40		3658.0	
		36580	80.03	3657	8:05.40			+2.5
		36579	80.00	3658	8:12.20			
		-	-	-	8:14.20	OFF		
		36540	80.03	3653	8:19.20			
		36552	80.00	3655	8:22.20		3654.0	
36535	79.97	3655	8:26					
18.0	50	36529	79.93	3656	8:42.00			
		36532	80.00	3653	8:50.00		3654.0	
		36551	80.03	3654	8:44.30			
		-	-	-	8:46.20	ON		
		36538	80.00	3654	8:53.10			
		36569	79.97	3658	8:56.10		3655.4	
		36549	80.03	3654	9:00.40			
36559	80.00	3656	9:03.20					
18.0	50	36562	80.03	3655	9:07.00			0
18.0	50	-	-	-	9:09.00	OFF		
		36562	79.97	3658	9:10.40			
		36558	79.97	3657	9:15.00		3657.0	

Continued

TABLE 1 (Continued)

Magnet Current (Amps)	Field (K Oe)	Counter			Time of Day	60 c/s AC current (22.5 A. rms)	Ave. Freq. (cy/sec)	Freq. Shift (cy/sec)
		Counts 8	Time (Seconds)	Freq. (cy/sec)				
14.6	40	36524	79.97	3654	9:24.40	OFF		
		36541	79.97	3656	9:27.00		3655.3	
		36583	80.03	3657	9:31.30			
		36543	80.00	3654	9:34			
		-	-	-	9:36.20	ON		
		36530	79.97	3654	9:38.00			
		36575	80.03	3656	9:44.00			
		36552	79.97	3654	9:49			
		36583	80.00	3654	9:50.40		3655.6	1.3
		31768	80.00	3177	9:54			
		43481	80.03	4347	9:56			
		32504	80.00	3250	9:58.50			
		36564	80.01	3656	10:03			
		-	-	-	10:03.40	OFF		
		36542	80.02	3653	10:04.40			
		36524	80.00	3652	10:08.30		3653.3	
		31712	79.93	3174	10:13			
		43470	80.06	4344	10:15.00			
		32525	80.02	3252	10:20			
		36545	79.99	3655	10:22.40			
3.5	10	36504	80.00	3650	10:40.30	OFF		
		36485	79.93	3652	10:43.00		3650.8	
		36528	80.06	3650	10:44			
		36522	80.02	3651	10:49			
		-	-	-	10:50.40	ON		
		36471	79.95	3649	10:53.40		3647.7	
		36468	80.02	3646	10:59			
		36461	79.97	3648	11:01.00			
-	-	-	11:03.00	OFF				
3.5	10	36480	80.04	3646	11:04.40	OFF		
		36530	79.98	3654	11:09.00		3651.3	-3.4
		36515	80.04	3650	11:14.10			
0	0	34240	80.00	3424	2:35 pm	OFF		
		34263	80.02	3425	2:57 pm			
		34290	80.03	3428	3:01.00		3424.3	
		34252	80.03	3424	3:03.00			
		34205	79.96	3422	3:06			
		34244	80.03	3423	3:07.30			
		-	-	-	3:10.40	ON		
		34241	79.99	3425	3:12.00			+0.3
		34247	80.01	3424	3:17		3424.3	
34249	80.03	3424	3:19.50					

Continued

TABLE 1 (Continued)

Magnet Current (Amps)	Field (K Oe)	Counter			Time of Day	60 c/s AC current (22.5 A. rms)	Ave. Freq. (cy/sec)	Freq. Shift (cy/sec)	
		Counts 8	Time (Seconds)	Freq. (cy/sec)					
0	0	-	-	-	3:21.50	OFF			
		34230	80.00	3423	3:23.00				
		34216	79.97	3423	3:36.40		3423.7		
		34249	80.00	3425	3:32.40				
3.5 3.500	10 10.0	-	-	-	3:35.00	OFF			
		34209	80.03	3420	3:46		3420.0	x	
		34186	79.97	3420	3:47.20				
		-	-	-	3:50.00	ON			
		34307	80.06	3428	3:53.40		3428.5		
		34298	80.03	3429	3:56.00			+1.2	
	3.500	10.0	-	-	-	3:58.00	OFF		
			34248	80.02	3424	3:59.00			
			34250	79.97	3426	4:01.00			
			34304	80.00	3430	4:04.00		3427.3	
			34285	80.00	3429	4:07.00			
			-	-	-	4:10.20	ON		
3.500	10.0	34278	79.98	3429	4:12.00				
		34310	80.03	3430	4:14.30		3429.3	+2.1	
		34292	80.00	3429	4:17.00				
		-	-	-	4:18.00	OFF			
		34270	80.00	3427	4:20.20		3427.0		
14.40	40	34243	79.96	3426	4:51	0			
		34248	79.99	3429	4:53.10		3426.3		
		34264	80.05	3424	4:55.10				
		-	-	-	4:57.20	10.0			
		34249	79.97	3426	4:58.40		3426.0		
		34257	80.00	3426	5:01.20			+0.6	
		-	-	-	5:03.20	0			
		34243	80.00	3424	5:06.10		3424.5		
		34276	80.06	3425	5:09.10				
		-	-	-	5:11.50	5.0			
		34248	80.00	3425	5:14.10		3426.0	+0.2	
		34260	79.97	3427	5:17.10				
-	-	-	5:17.40	0					
34270	80.00	3427	5:19.30		3427.0				
34272	80.00	3427	5:22.00						
3.50	10	34257	80.03	3424	5:37.50	0			
		34234	79.97	3425	5:40.20		3424.5		
		-	-	-	5:43.00	5.0			
		34270	80.03	3426	5:44				
		34283	80.00	3428	5:46.10				
		34263	80.00	3426	5:50.10		3427.0		

Continued

TABLE 1 (Continued)

Magnet Current (Amps)	Field (K Oe)	Counter			Time of Day	60 c/s AC current (22.5 A. rms)	Ave. Freq. (cy/sec)	Freq. Shift (cy/sec)
		Counts 8	Time (Seconds)	Freq. (cy/sec)				
		34282	80.00	3428	5:53.00			-2.4
		-	-	-	5:55.00	0		
		34265	79.98	3427	5:55.45			
		34295	80.00	3430	5:58.40			
		34340	80.03	3433	6:01.00		3434.4	
		34377	80.00	3438	6:03.30			
		34326	80.02	3432	6:06.00			
		34323	79.98	3433	6:07.50			
		34318	80.02	3431	6:10.20			

TABLE 2

Quench Currents of Spot Welded and Cold Worked Joints in Nb 25 Zr Wire

Sample	Magnet		Superconducting to Normal (Quench) Currents		
	Current (Amps)	Field (K Oe)	1st Run (Amps)	2nd Run (Amps)	3rd Run (Amps)
Spot weld:	0	0	100	98	112
9 watt-sec	3.5	10.	20	18	18
Cold work:	7.1	20.	9	9	9
1560. gm-cm	10.5	30.	7	7	7
	13.8	39.	5	5	5
	15.9	44.	5	5	5
Spot weld:	0	0			
9 watt-sec	3.5	10.	18	17	17
Cold work:	7.1	20.	8	9	9
3130. gm-cm	10.5	30.	8	8	8
	13.8	39.	5	6	6
	15.9	44.	5	5	5
Spot weld:	0	0	< 1.	< 1.	< 1.
4.5 watt-sec	3.5	10.	< 1.	< 1.	< 1.
Cold work:	10.4	29.	< 1.	< 1.	< 1.
0. gm-cm					
Spot weld:	0	0	102	102	104
9 watt-sec	3.5	10.	11.	11.	11.0
Cold work:	7.1	20.	6	7	6
0. gm-cm	10.5	30.	4	4	4
	13.8	39.	4	4	4

is that gas law thermometric measurements can be made to corroborate sonic thermometer data.

Calibration of temperature versus frequency was performed by measuring the sonic cavity resonant frequency while the calorimeter was immersed in liquid helium at various vapor pressures (see Table 3).

Comparison of the frequency shift data with those of Itterbeek et al. (11, p. 63) shows a shift of approximately 1/3 of their values. This difference is due to a relatively large dead volume in the probe used in the tests for this thesis.

Using the data of Table 4, the temperature rise of the helium gas inside the sonic resonance space was computed as 0.03°K with a standard input signal of 10,000 cycles/sec.

Results of the almost isothermal calorimeter measurements are given in the results section.

TABLE 3

Temperature and Pressure Calibration of Almost Isothermal Calorimeter [Compared with Data of Itterbeek et al. (1)]

Probe Pressure (mm, Hg)	Dewar Temp.		Counter			Velocity ($\frac{\text{meters}}{\text{sec}}$)	V/freq. (meters)	
	Pressure (mm, Hg)	$^{\circ}$ K	$\frac{\text{Counts}}{8}$	Time (seconds)	Freq. (cy/sec)			
152.	756.9	4.21	8467.8	79.97	8471	118.0	.01390	
	756.9	4.21	8491.9	80.00	8492	118.0	.01390	Best value
	479.4	3.76	8444.4	80.00	6444	111.2		
	479.4	3.76	8404.8	79.93	8412			
	479.4	3.76	8416.8	80.06	8411		.01323	
	479.4	3.76	7909.0	80.06	7903		(.01407)	Lower side band
	515.0		8957.9	80.03	8955		[.01242]	Upper side band
	756.9	4.21	8965.8	80.04	8962	118.0	[.01317]	Upper side band
	756.9	4.21	8491.6	80.03	8489		.01390	Main peak
	756.9	4.21	8453.1	80.00	8453			Main peak
			8009.1	79.99	8010		(.01475)	Lower side band
	304.	756.9	4.21	7929.8	80.00	7930	115.0	(.01450)
			8382.7	80.02	8381		.01373	Main peak
			8428.5	77.96	8433		.01366	Main peak
			8962.4	80.03	8899		[.01289]	Upper side band
			8900.6	79.97	8904		[.01292]	Upper side band

TABLE 4

Temperature Rise of Almost Isothermal Calorimeter Due to Standard 10 KC Input

Counts	Counter		Ave. Freq. (cy/sec)	Helium Pressure in Probe (mm, Hg)	Time of Day	AC input to Super conductor	Freq. Shift (cy/sec)
	Interval (seconds)	Freq. (cy/sec)					
8							
81707	80.02	8167	8168.0	396	6:02	OFF	
81720	80.03	8169			6:03		
82118	79.99	8213	8212.5	375	6:05	ON	42.
82045	79.93	8212			6:07		
81783	80.03	8175	8172.5	388	6:11	OFF	
81757	80.06	8170			6:14		

$$p \doteq 394 \text{ mm} = 0.518 \text{ ATM}$$

$$p \doteq 375 \text{ mm} = 0.493 \text{ ATM}$$

Referring to Itterbeek (1, p. 63)

At 4.228°K. the pressure difference gives a velocity ratio of $\frac{112.7}{113.3} = .993$. The frequency ratio observed is $\frac{8170.3}{8212.5} = .995$. The temperature rise is seen then from their graph to be less than 0.03°K.

RESULTS

Theoretically Predicted Heat Loss Calculation

The data of Kim et al. is used on a 3NbZr sample placed perpendicular to the field and given values of H' versus H from their data in Figure 1 (7, p. 534).

Table 5. Magnetization Data from Kim et al.

H' in(KOe) up	H'_1 in(KOe) down	H in KOe
+2.1	-2.4*	-0.5
+2.6	-1.8*	+0.5
+4.2	+2.1	+3.2
+4.6	+2.8	+3.7
+6.3	+5.2	+5.8
+3.9	+1.2	+2.7
+3.1	-1.0	1.5
+2.4	-2.1*	0.0

* Deduced from horizontal folding symmetry

The values of $(\Delta H'/\Delta H)^2$, as shown in Table 6, were computed from the data at magnetic field intensities of 6.0, 3.2, 2.1, 1.0, and 0.0 KOe.

Almost Isothermal Calorimeter

From the data on 3NbZr wire (Table 7) held transverse

Table 6. Alternating Field Energy Loss-versus-Magnetic Field. Calculation from Data in Table 5.

H(KOe)	$\Delta H'$ up	ΔH up	$\Delta H'/\Delta H$ up	W up	$\Delta H'$ down	ΔH down	$\Delta H'/\Delta H$	W down	W average (arbitrary units)	W overall average
0.0	0.5	1.0	0.50	0.25	0.5	1.0	0.50	0.25	0.25	0.3
0.0 ⁻	0.3	0.5	0.60	0.36	0.2	0.5	0.40	0.16	0.26	
0.0 ⁺	0.2	0.5	0.40	0.16	0.3	0.5	0.60	0.36	0.26	
3.2	0.7	1.0	0.70	0.49	1.6	1.0	1.60	2.56	1.53	1.6
3.2 ⁻	0.4	0.5	0.80	0.64	0.9	0.5	1.80	3.24	1.94	
3.2 ⁺	0.4	0.5	0.80	0.64	0.7	0.5	1.40	1.96	1.30	
6.0	1.0	1.0	1.00	1.00	1.0	1.0	1.00	1.00	1.00	1.0
1.0	0.5	1.0	0.50	0.25	0.8	1.0	0.80	0.64	0.45	
1.0 ⁻	0.2	0.5	0.40	0.16	0.4	0.5	0.80	0.64	0.40	0.5
1.0 ⁺	0.3	0.5	0.60	0.36	0.4	0.5	0.80	0.64	0.50	
2.1	0.8	1.2	0.67	0.45	2.3	1.2	1.92	3.69	2.07	
2.1 ⁻	0.4	0.6	0.67	0.45	1.0	0.6	1.67	2.79	1.62	2.0
2.1 ⁺	0.4	0.6	0.67	0.45	1.2	0.6	2.00	4.00	2.23	

TABLE 7

Almost Isothermal Calorimeter

Time of Day	Probe Pressure		Change of Probe Pressure (mm, Hg)	Counter			Current (Amps)	Field (K Oe)	AC to Sample			
	(ATM)	(mm, Hg)		Counts 8	Duration (seconds)	Freq. (cy/sec)			Freq. (KCS)	Volts at		Amps
										Out	Ampl.	
3:20 pm		163.0		84714	80.03	8368	0	0				
	.20	152.5	-	84761	80.03	8473	0	0	0	0		
3:34		152.5	4.4	84409	80.03	8437	0	0	10	1.65		
3:36		152.5	-	84653	80.02	8463	0	0	0	0		
3:39		152.5	5.0	84646	80.00	8465	0	0	10	1.65		
4:02		150.9	-	84572	79.98	8459	3.50	10.	0	0		
		152.0	4.0	84570	80.00	8457			10	1.65		
		152.5	-	84566	80.04	8453	0	0	0			
4:21		152.5	4.2	84311	79.97	8434	10.60	30.	10	1.65		
		152.5	-	83826	79.97	8386	1.03	3.2	0	0		
		152.5	3.6	83989	80.05	8404		1	10	1.65		
						0	0					

to the external field, the following frequency shifts which can be assumed directly proportional to power loss for the small temperature changes are obtained. Also the change of pressure of the system was read with a mercury manometer and these values are entered as corroborative data:

Table 8. Heat Losses for Almost Isothermal Calorimeter.

Field (KOe)	ΔP (mm Hg)	$\Delta \text{freq.}$ (cy/ sec)	W theor (Kim <u>et al.</u>)	W / ΔP (ratio)	W / $\Delta \text{freq.}$ (ratio)
0.0	4.4	---	0.22	0.05	----
0.0	5.0	4.	0.22	0.04	0.06
10.0	4.0	1.	1.00	0.25	1.00
3.2	3.6	18.	1.70	0.47	0.09

Since the units of W are arbitrary the correspondence of theory and experiment is indicated by the constancy of W / ΔP and W / $\Delta \text{frequency}$ values.

The wide variation between results of manometer readings and the sound velocity implies a poor localization of the heat source to the sample. Curves of Itterbeek and de Laet (11, p. 63) show that at probe pressure at 0.20 ATM a change of 5. mm Hg $\frac{5}{1013.25} = 0.0066$ ATM would cause change of sound velocity less than 0.1 percent at 4.2°K. The observed frequency shifts were all less than

$\frac{18}{8500}$ (100%) = 0.2 percent, thereby indicating that the observed frequency shifts were due largely to the heating of the gas in the probe system by the lead-in wire rather than localized heating of the sonic thermometer by the superconducting wire which would cause very little system pressure rise.

Adiabatic Calorimeter

The results of frequency shift can be assumed linearly related to a-c heat loss for small frequency shifts. Using arbitrary units for calculated theoretical heat loss we compute the ratio of calculated loss to measured frequency shift and establish the degree of correspondence of the shape of loss-versus-field curve.

Table 9. Heat Losses for Adiabatic Calorimeter.

Field (KOE)	Δ freq (cy/ sec)	Δ W theor (arbitrary)	Ratio (W / Δ f)
0.0	6.	0.22	0.03
10.	- .6	1.00	0.50
20	2.5	1.00	0.50
40	0.7	1.00	1.00

The experimental data are compared with the theory in Figure 6. The maximum of heat loss as the field passes through

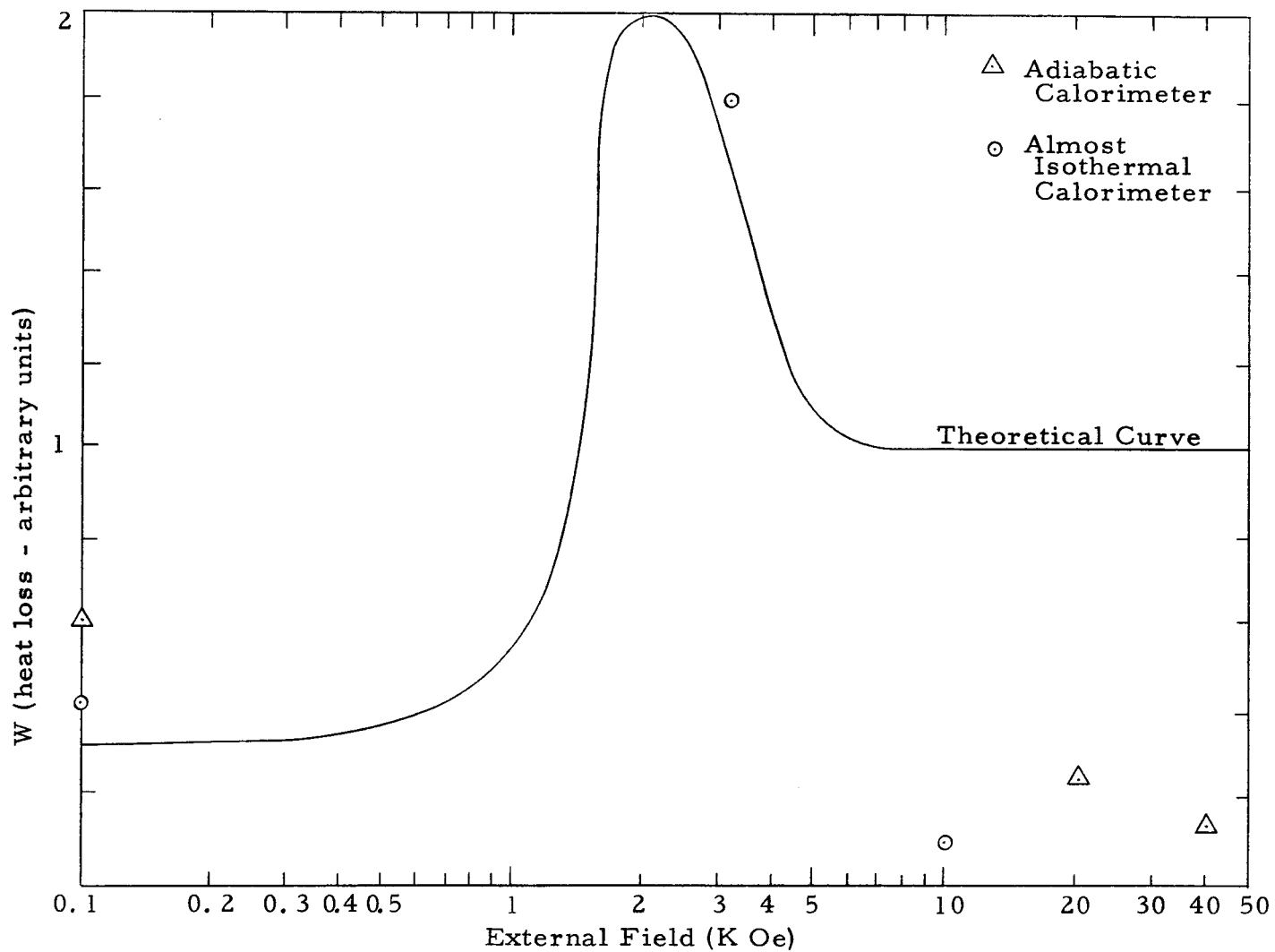


Figure 6. Comparison of Theory with Experimental Data.

2 KOe in Nb₂₅Zr wire corresponds to the maximum slope of the magnetization curve averaged over ascending and descending paths.

CONCLUSIONS

Sensitivity, although marginal, is sufficient to indicate general agreement of results with critical state theory predictions of Bean (3) and Kim et al. (7).

Results were not compared to predictions of GLAG theory (5, p. 6) modified by Anderson (2), Goodman (6), or Silcox and Rollins (10) because of difficulty in reducing the theories to a prediction of heat loss expected.

Note the indication of lower losses above 10 KOe which implies that an a-c device operating at a d-c bias may have less hysteretic losses.

RECOMMENDATIONS

Sensitivity is limited in this experiment by the experimental volume available in the superconducting magnet. A further effort should be made to make more accurate measurements in a one inch bore or larger magnet.

Application of accurate measurements to the modified GLAG theory would be of fundamental value in establishing whether the loss-versus-field properties are those to be predicted by the vortex lattice of Abrikosov which interacts with lattice defects, or that predicted by the critical state theory as here remarked.

Further material studies are proposed to develop materials which can be operated at a magnetic bias and for which the a-c loss mechanism may be minimized.

BIBLIOGRAPHY

1. Abrikosov, A. A. On the magnetic properties of superconductors. Soviet Physics JETP 5:1174-1182. 1957.
2. Anderson, P. W. Theory of flux creep in hard superconductors. Physical Review Letters 9:309-311. 1962.
3. Bean, C. P. Magnetization of hard superconductors. Physical Review Letters 8:250. 1962.
4. Friedel, J., P. G. deGennes, and J. Matricon. Nature of the driving force in flux creep phenomena. Applied Physics Letters 2:119-121. 1963.
5. Ginzburg, V. L. and L. D. Landau. A theory of superconductivity. Zhurnal Eksperimental'noi i Teoreticheskoi Fiziki 20:1064-1082. 1950 (Translated as AEC-tr-1395)
6. Goodman, B. B. Simple model for the magnetic behavior of superconductors of negative surface energy. Physical Review Letters 6:597. 1961.
7. Kim, Y. B., C. F. Hempstead and A. R. Strnad. Magnetization and critical supercurrents. Physical Review 129:528-535. 1963.
8. Mendelssohn, K. A discussion on supraconductivity and other low temperature phenomena. Proceedings of the Royal Society, London 152:34-41. 1935.
9. Morin, F. J. et al. Heat capacity evidence for a large degree of superconductivity in V_3Ga in high magnetic fields. Physical Review Letters 8:275-278. 1962.
10. Silcox, J. and R. W. Rollins. Hysteresis in hard superconductors. Applied Physics Letters 2:231-233. 1963.
11. Van Itterbeek, A. and W. de Laet. Measurements on the velocity of sound in helium gas at liquid helium temperatures. Physica 24:59-67. 1958.
12. Zar, Jacob L. Measurement of low resistance and the a-c resistance of superconductors. Review of Scientific Instruments 34:801-804. 1963.